Journal of Molecular Structure 1056–1057 (2014) 299–306

Contents lists available at ScienceDirect

Journal of Molecular Structure

journal homepage: www.elsevier.com/locate/molstruc

Enhanced processability of MWCNT through surface treatment by octa(phenol) polyhedral oligomeric silsesquioxane nano-crosslinking

Abdollah Omrani [a,b,*], Ying-Chieh Yen [a], Chih-Chia Cheng [a], Feng-Chih Chang [a]

[a] Institute of Applied Chemistry, National Chiao-Tung University, Hsin-chu, Taiwan
[b] Faculty of Chemistry, University of Mazandaran, P.O. Box 453, Babolsar, Iran

HIGHLIGHTS

- OP-POSS was used as a novel cross-linker for MWCNT.
- The processability of MWCNT enhanced by the POSS presence.
- WAXD study confirmed an amorphous structure for MWCNT–POSS nanocomposite.

ARTICLE INFO

Article history:
Received 18 June 2013
Received in revised form 19 October 2013
Accepted 21 October 2013
Available online 26 October 2013

Keywords:
Surface treatment
MWCNT
Nanocross-linking
Octa(phenol) polyhedral oligomeric silsesquioxanes
Esterification

ABSTRACT

A facile method was developed to prepare MWCNT/POSS nanocomposites by direct esterification between carboxylic acid functionalized MWCNT and octa(phenol) octasilsesquioxane. Completeness of the MWCNT surface modification was confirmed by FT-IR. The hybrid nano-MWCNT–OP-POSS composite structure and properties was characterized using DSC, TGA, optical microscopy, WAXD, and AFM. The results indicated the solubility and processability of MWCNT–COOH improved because of OP-POSS grafting on MWCNT surface. The T_g and thermal stability of the nanocomposites was higher than that of the OP-POSS as a result of the cross-linking reaction. AFM observations revealed that the nanocomponents were reacted in a homogeneous phase at nanoscale level.

1. Introduction

Over the past decade, polyhedral oligomeric silsesquioxanes (POSSs) have attracted intensive interest as self-healing high-temperature nanocomposites and space-survivable coatings [1,2] low-k dielectric materials [3], and as templates for the preparation of nanostructured materials such as liquid crystalline polymers [4], catalysts [5,6], and optoelectronics [7]. Cage siloxanes consisting of POSS or spherosilicates denote inorganic–organic hybrid molecules having cage-like Si_8O_{12} cores and substituents attached to each vertex of the core [8–11], and they have been widely used as excellent platforms for producing new hybrid materials [12–15], as supports for organometallic catalysts [16–18], and even as anion receptors [19,20]. It is worthy to note that via appropriate design of the functionalities on carbon surface, many new and potentially valuable applications will be provided. Recently, several octafunctionalized POSS bearing functional groups such as methacrylates [21], epoxies [22], alcohols [23], and isocyanate [24] have been synthesized and studied. To improve the versatility, non-hydrosilylation based techniques were also employed to synthesize new POSS derivatives [25–30].

On the other hand, carbon nanotubes (CNTs) possess remarkable electrical (such as electric-current-carrying capacity 1000 times higher than copper wire), thermal and mechanical properties, allowing a number of exciting potential applications, and leading them to be potential candidates for manufacturing advanced hybrid materials. To modify CNTs, numerous functionalizations and fabrications have been studied [31–39]. As mentioned earlier, POSS and its derivatives are emerging as a new chemical technology owing to simplicity in processing, excellent mechanical properties, thermal stability, and flame redundancy. According to our knowledge, there were limited reports regarding hybrid nanostructures from MWCNT and POSS or its derivatives [40]. The pre-modification of MWCNTs resulted in influence on their properties because the reaction may destroy the structure of MWCNT. The motivation for the present research is to construct new nanobuilding blocks through custom-designed organic functionality according to a green method. The OP-POSS reported previously was reacted with

* Corresponding author at: Faculty of Chemistry, University of Mazandaran, P.O. Box 453, Babolsar, Iran. Tel.: +98 5342383; fax: +98 5342350.
E-mail address: omrani@umz.ac.ir (A. Omrani).

0022-2860/$ - see front matter © 2013 Elsevier B.V. All rights reserved.
http://dx.doi.org/10.1016/j.molstruc.2013.10.053

carboxyl acid groups on the surface of a commercialized MWCNT through esterification only by heating and the completeness of the esterification reaction was verified by the FTIR spectroscopy. The thermal properties of the nanocomposites were investigated through DSC and TGA measurements, and the WAXD measurement was employed to observe their microstructures.

2. Experimental

2.1. Materials

Acetone, tetrahydrofuran (THF), platinum divinyl tetramethyldisiloxane complex [Pt(dvs)], 4-acetoxystyrene (AS) were purchased from Aldrich Chemical Co. Q8M8H, $C_{16}H_{56}O_{20}Si_{16}$, was obtained from Hybrid Plastics Co. The MWCNT–COOH with a diameter (OD) of 20–30 nm, a length of 10–30 microns, and a purity (wt%) >95% was obtained from Chengdu Organic Chemicals Co. Ltd., Chinese Academy of Sciences. The materials were used as received without further purification. Octa(phenol) octasilsesquioxane (OP-POSS) was synthesized and characterized according to the method described previously [41].

2.2. Characterizations

FTIR measurements were made over the range 4000–400 cm^{-1} using a Nicolet Avatar 320 FT-IR Spectrometer, 32 scans at a resolution of 1 cm^{-1}. Wide angle X-ray diffraction (WAXD) measurements were carried out using a Bruker Nanostar U System, with incident X-ray radiation source which is Ni-filtered Cu Kα radiation at a wavelength (λ) = 0.1542 nm. The voltage and current were set at 30 kV and 20 mA, respectively. The collimation system consisted of two cross-coupled Gobel Mirrors and four pinholes. A Histar area detector (Siemens) filled with pressurized xenon gas was used to record the WAXD scattering patterns, with a sample to detector distance of 3 cm, respectively. All WAXD measurements were performed at room temperature and the data were monitored using a proportional counter detector over the 2θ range of 4–40°. A DuPont thermal gravimetric analyzer (TGA Q100) was employed to investigate the thermal stability of the MWCNT nanomaterials. The sample (about 5 mg) was heated from ambient temperature to 800 °C in a nitrogen atmosphere with a heating rate of 20 °C/min. Differential scanning calorimetry (DSC) studies were carried out with a DuPont TA 2010 DSC calorimeter under nitrogen atmosphere (50 cm^3/min) at scan rate of 20 °C/min from room temperature to 210 °C. The samples re-heated at 5 °C/min from −70 to 200 °C to minimize the relaxation enthalpy and to determine the residual heat. The glass transition temperature (T_g) was obtained as the inflection point of the heat capacity jump. Atomic force microscopy (AFM) data on height measurements of the cured nanocomposites were acquired using a tapping-mode AFM (Digital Instrument NS4/D3100CL/Multi-Mode AFM; Veeco-Digital Instruments, Santa Barbara, CA) having silicon cantilevers (Pointprobe Silicon AFM Probe) at room temperature, in air. Damage to both the tip and the sample surface were minimized by employing the AFM in tapping mode.

2.3. Sample preparations

Samples of OP-POSS/MWCNT–COOH with 10 wt%, 25 wt%, 40 wt%, 50 wt%, and 60 wt% of MWCNT–COOH were prepared. The OP-POSS was dissolved in THF (10 ml) for 30 min with stirring and then desired amount of MWCNT–COOH added to the solution. The reactants were stirred vigorously for 8 h at room temperature to disperse MWCNT homogeneously. Finally, the dark suspension was vacuum-filtered and then washed with THF to remove unreacted OP-POSS. The solid product was dried in vacuum oven at 60 °C for 12 h. These blends were safely kept in a refrigerator at 4 °C prior to the DSC measurements.

2.4. Sample preparation for spectroscopic and morphology investigations

The same method as described above was utilized to prepare OP-POSS/MWCNT–COOH blends. The dried blends were cross-linked in vacuum at 120 °C for 4 h and then post-cured at 150 °C for an additional 2 h. The post-curing treatment was imposed to make sure that most functional groups of the reactants have been involved in the esterification reaction. The powdered samples were used for the TGA and XRD tests. A spin coating deposition technique was used to prepare the samples for optical microscopy and AFM observations. About 4–5 drops of the homogeneous blends in THF was placed on micro cover glasses to produce very thin films of the compositions and then cured according to the described curing cycle. For FTIR measurement, the blend samples were prepared on KBr pellets.

3. Results and discussion

3.1. Grafting of OP-POSS onto MWCNT

Fig. 1 is a schematic representation of our approach to cross-linking of MWCNT using OP-POSS. The esterification reaction between hydroxyl groups of OP-POSS and carboxyl acid groups of MWCNT–COOH was carried out by heating of the blends at high temperature. After the reaction, the hydroxyl groups of OP-POSS will be converted into ester units as well. The effectiveness of the esterification reaction was demonstrated by FTIR spectroscopy.

Fig. 2 confirms that the degree of conversion of hydroxyl group depends on the concentration of MWCNT–COOH. Obviously, as the content of MWCNT–COOH increases, the peak intensity of Si–OH at 917 cm^{-1} decreases, correspondingly [42,43].

TGA curves of the MWCNT–COOH, OP-POSS, and nanocomposites with various compositions are shown in Fig. 3. There is ca. 2.7% weight loss of the pristine MWCNT–COOH from 100 to 500 °C owing to the possible organic and solvent impurities trapped in it.

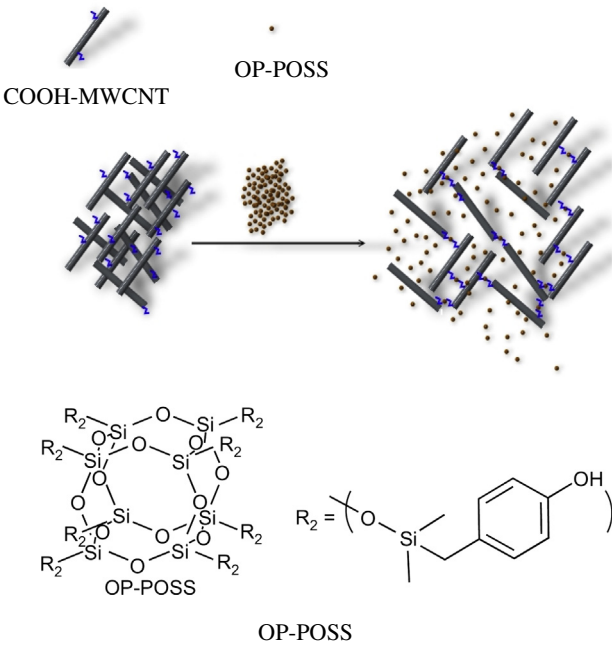

Fig. 1. Schematic representation of the MWCNT–COOH cross-linking.

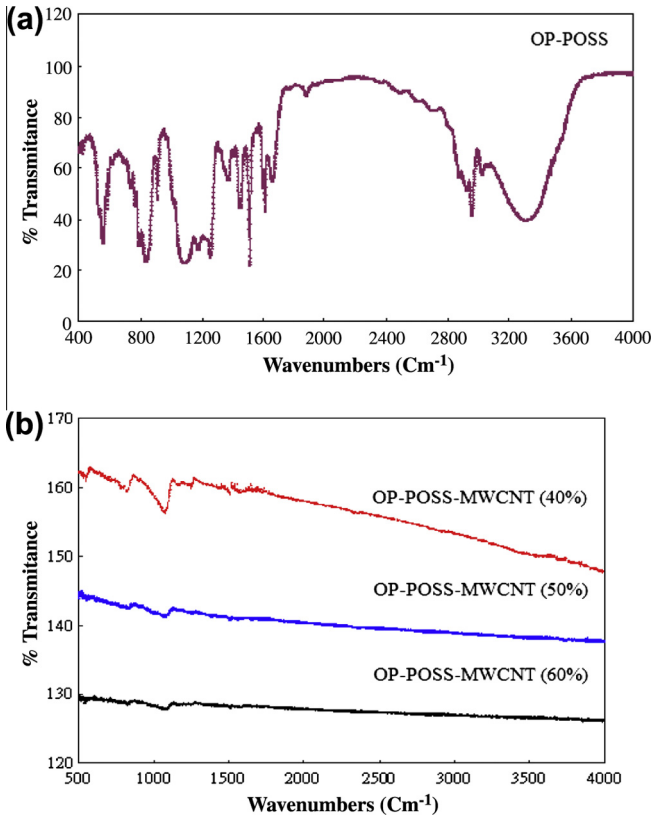

Fig. 2. FT-IR spectra of (a) OP-POSS and (b) cured nanocomposites.

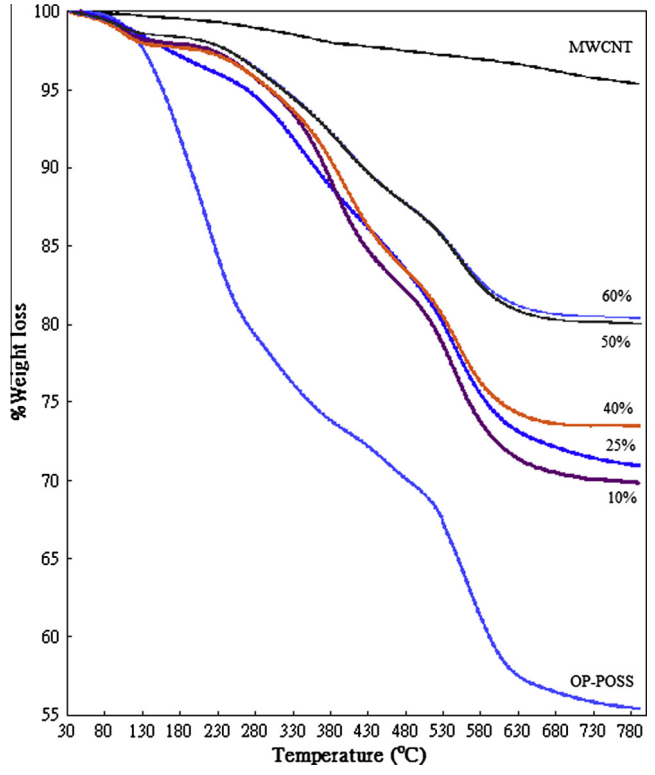

Fig. 3. TGA traces of MWCNT–COOH and OP-POSS grafted MWCNT at various concentrations.

This also could result from the defects on the MWCNT surface. A relatively slow loss in mass (2%) up to 800 °C at which the value of residue is ca. 95.3% was observed. At 500 and 800 °C, the OP-POSS showed the residues of 69.3% and 55.4%, respectively. However, the nanocomposites possess sustainable thermal stability as evidenced by the TGA curves shown in Fig. 3. The residue of the nanocomposite having 10 wt% of MWCNT–COOH at 800 °C is ca. 70%. Upon increasing the MWCNT–COOH content within the POSS/MWCNT–COOH composites, the decomposition temperature and the residue of the composites are increased because of the presence of cross-linkage and MWCNT–COOH. By assuming that at 750 °C the MWCNT–COOH residue remaining in the nanocomposites has the same wt% as that of the sole MWCNT–COOH, and with considering that the wt% of OP-POSS at 750 °C is equal to 55.6%, the wt% of MWCNT in the resulting nanocross-linked structures can be determined. For example, the nanocomposite involving 10 wt% MWCNT shows a residue of 69.9% at 750 °C which actually demonstrate that the amount of OP-POSS grafted onto MWCNT is about 9.9% based on the total weight of the sample. This method of analysis allows estimating the level of OP-POSS grafted onto the MWCNT surface. The result of this analysis was summarized in Table 1.

Table 1
The value of OP-POSS grafted (%) onto MWCNT surface calculated by TGA and a solution test method.

Nanocomposite	TGA method (%)	Solution test method (5)
OP-POSS–MWCNT (10%)	9.9	10.7
OP-POSS–MWCNT (25%)	11.2	12
OP-POSS–MWCNT (40%)	13.5	13.9
OP-POSS–MWCNT (50%)	20	21.2
OP-POSS–MWCNT (60%)	20.4	22

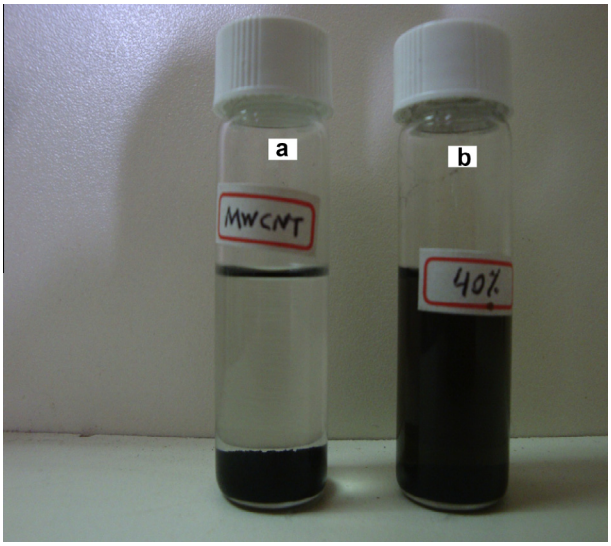

Fig. 4. Comparison of the samples solubility in acetone at 25 °C: (a) MWCNT–COOH. (b) OP-POSS-MWCNT (40%) blend. The black dispersion in (b) was stable for 1 month.

The attachment of OP-POSS on the MWCNT surface is further confirmed by a simple chemical treatment. Accordingly, a solution based quantitative approach was employed to estimate the level of cross-linking in the nanocomposites. An exact value of the cross-linked sample was dispersed in acetone by vigorous stirring at room temperature for 8 h to dissolve the un-reacted OP-POSS after curing. The resulting homogeneous solution was quickly filtered and then washed two times by 10 ml of THF. Finally, the residue was dried in a vacuum oven at 120 °C to remove the solvents. By considering the initial weight of the samples and the fact that

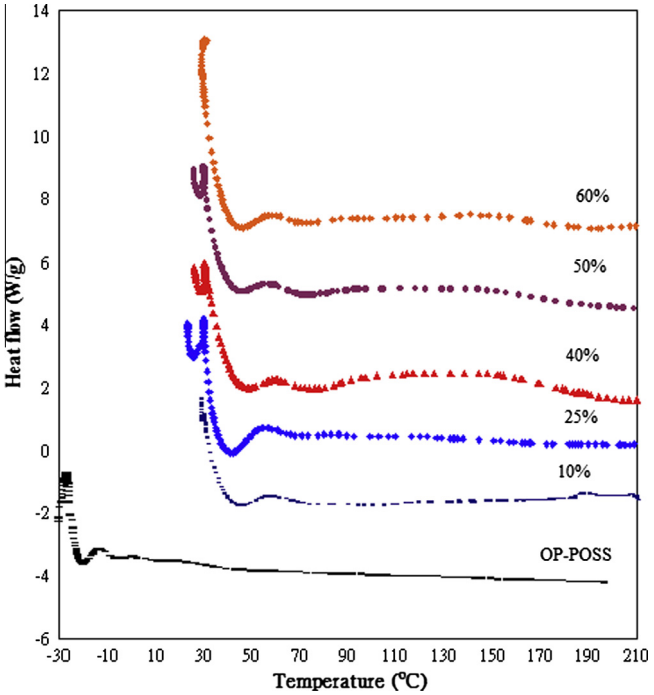

Fig. 5. DSC thermograms of OP-POSS and various OP-POSS/MWCNT nanocomposites at 20 °C/min.

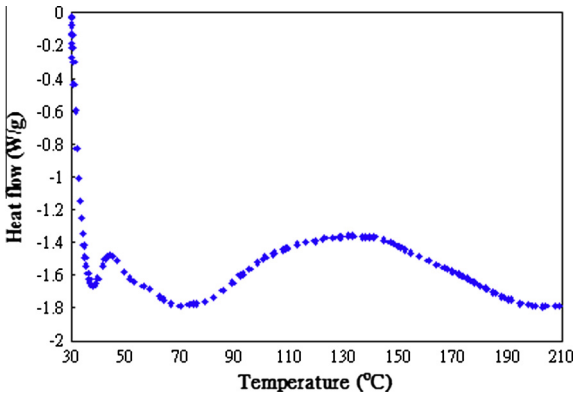

Fig. 6. DSC curve of OP-POSS/MWCNT (40%) nanocomposite cured at 10 °C/min in nitrogen atmosphere.

MWCNT–COOH cannot be dissolved in acetone and THF, the content of cross-linked OP-POSS was determined and summarized in Table 1. The content of cross-linked product is increased with the increase in the content of MWCNT–COOH, reflecting the consequence obtained from TGA.

In addition, when these OP-POSS/MWCNT–COOH blends are dispersed in acetone before curing, both solubility and processability of MWCNT–COOH in organic solvents are substantially improved. As shown in Fig. 4, a stable dispersion can be obtained which indicates the specific role of OP-POSS in dispersing MWCNT–COOH. The stability of the MWCNT–COOH within the uncross-linked OP-POSS/MWCNT–COOH blends strongly depends on the content of OP-POSS within the blends, implying that OP-POSS plays a role as compatibilizer between MWCNT–COOH and acetone. However, stability of the OP-POSS/MWCNT dispersions is affected by efficiency of the esterification reaction. That means, it does depend on the degree of cross-linking or level of grafting. Fig. 4 exhibits that all of MWCNT

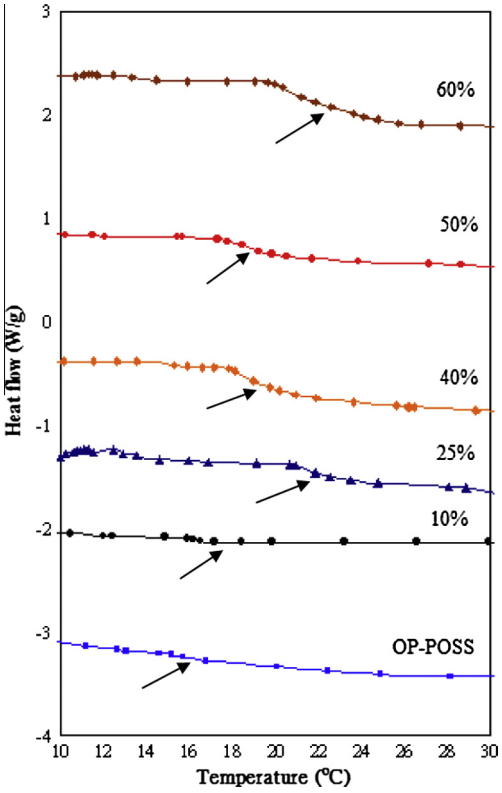

Fig. 7. DSC thermograms depicting T_g's of OP-POSS and the nanohybrids containing different MWCNT percentages.

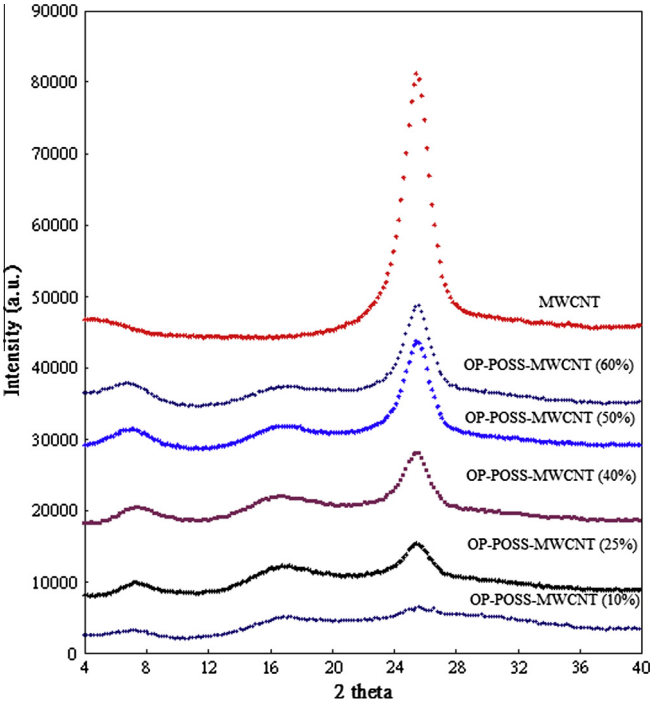

Fig. 8. WAXD profiles of the neat MWCNT–COOH and the nanostructured networks.

sank in acetone while the grafted nanostructure has higher degree of miscibility owing to the presence of OP-POSS on the MWCNT surface.

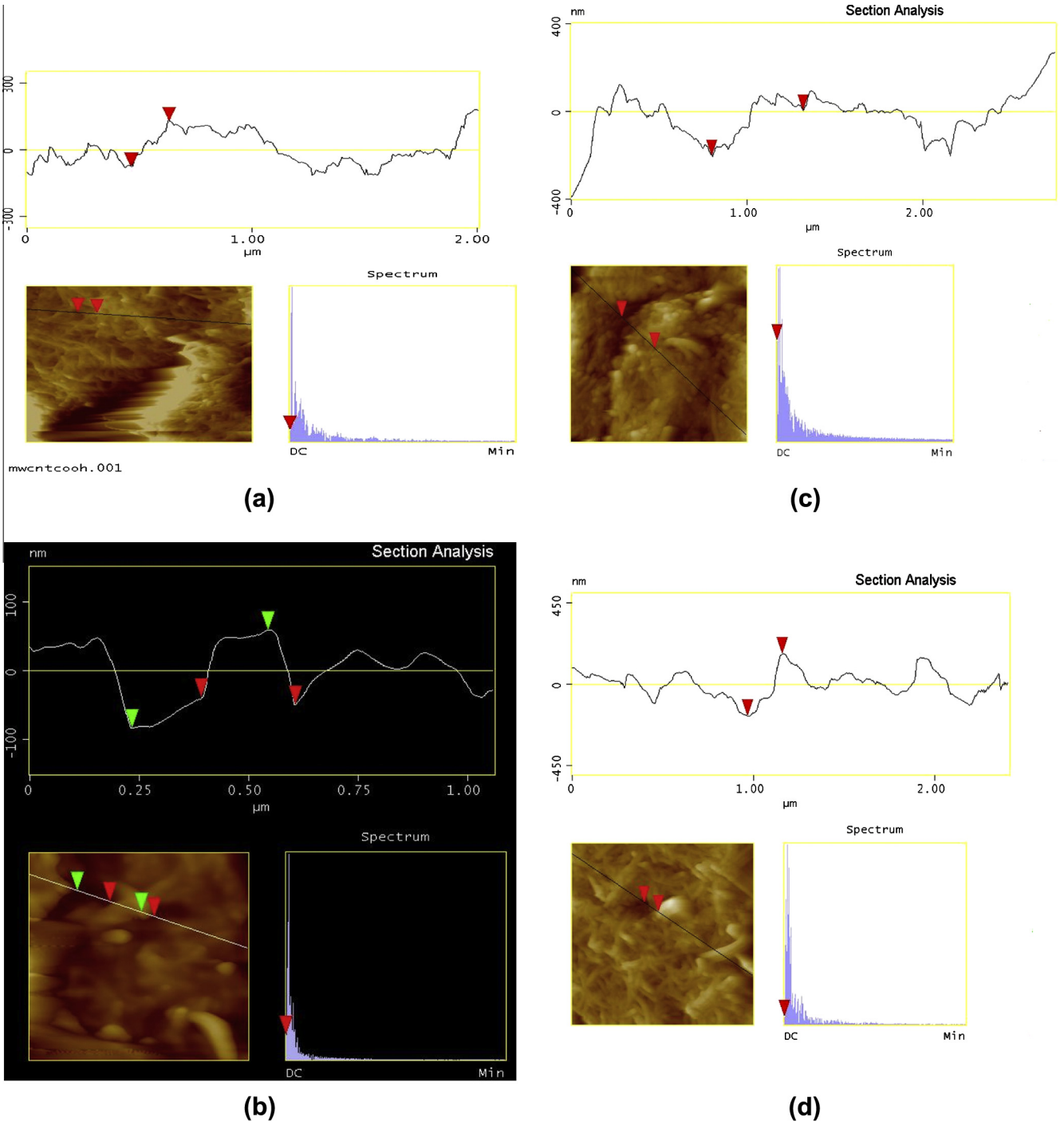

Fig. 9. Typical AFM images of (a) the neat MWCNT and its nanocomposites with OP-POSS at various compositions: (b) MWCNT (10%), (c) MWCNT (40%), and (d) MWCNT (60%).

3.2. Evidences for nanocross-linking reaction from DSC studies

Differential scanning calorimetry was used to observe the cross-linking reaction between OP-POSS and MWCNT–COOH. The cross-linking profiles of neat OP-POSS and OP-POSS/MWCNT nanocomposites are shown in Fig. 5.

Clearly, there are no signals for the pristine OP-POSS within the selected temperature range. Without any catalyst, the cross-linking peak temperature of the nanocomposite having 40 wt% of MWCNT lies between 75 to 200 °C. When the nanocomposites have relatively lower concentrations of MWCNT–COOH such as 10 and 25 wt%, the exotherm was unclear since the concentration of COOH functionality of MWCNT–COOH is quite low. For all these OP-POSS/MWCNT–COOH nanocomposites, only one broad exothermic peak is observed in each case, which demonstrates that a one-step reaction is the main process of the system under study. In addition, two or three distinct exothermic peaks can be observed if a curing reaction possesses two or three stages with considerable differences in the activation energies. Therefore, observing only one exothermic peak can be described by the esterification reaction between these functional groups on OP-POSS and MWCNT–COOH. With the increase in the curing time or temperature, the

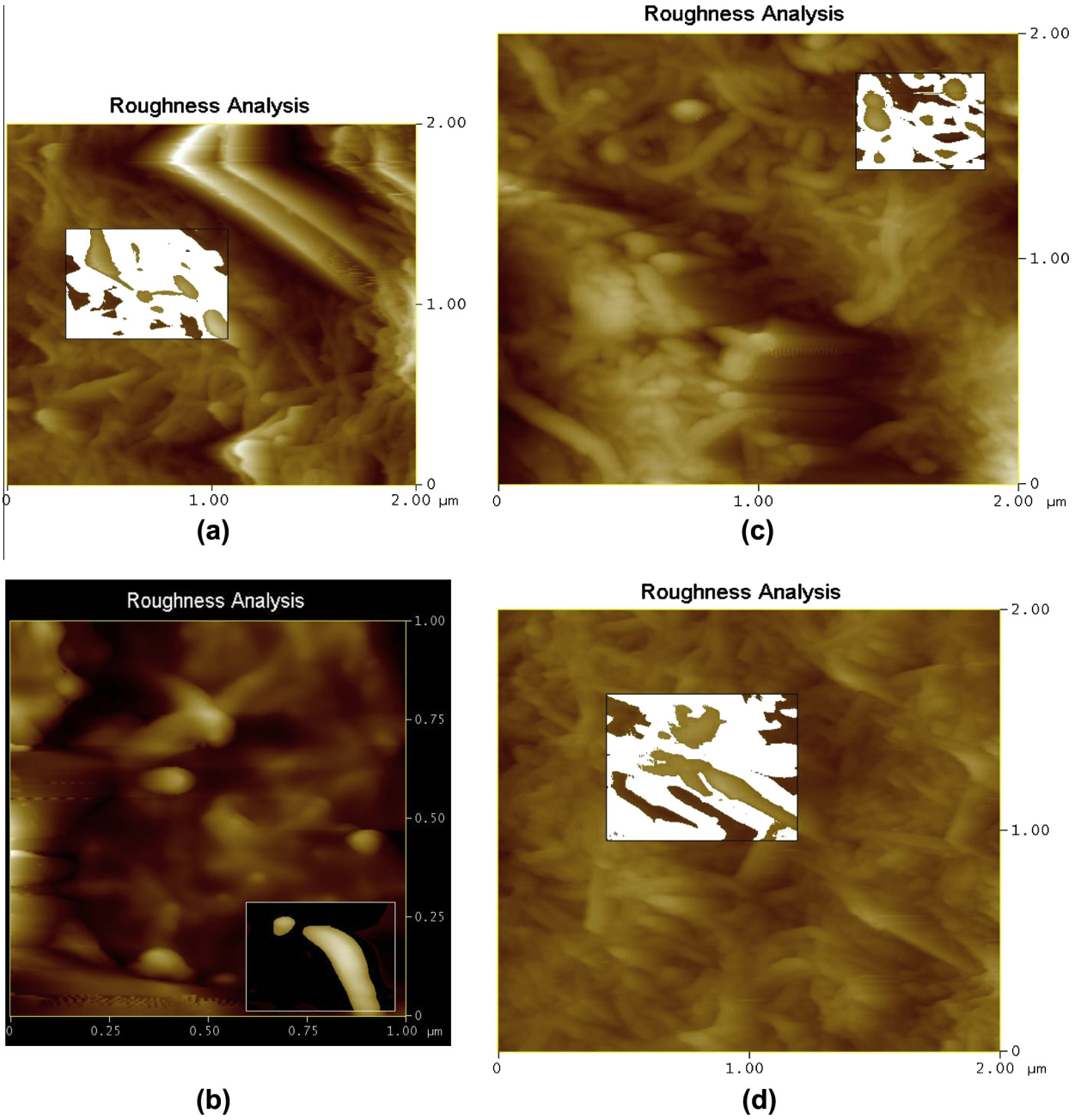

Fig. 10. Typical AFM images on roughness analysis of (a) the neat MWCNT and its nanocomposites with OP-POSS at various compositions: (b) MWCNT (10%), (c) MWCNT (40%), and (d) MWCNT (60%).

steric factor for these reacting functionalities will be increased as a result of cross-linking reaction but free functionalities are still available for further reaction. Thus, the observed broad exothermic peak is due to the gradual evolution of heat.

Further characterization of the cross-linking reaction was achieved by examining the nanocomposite having 40 wt% of MWCNT using DSC at a lower heating rate (10 °C/min). As shown in Fig. 6 the obtained exothermic peak is different from that observed at scan rate of 20 °C/min and at the same temperature range demonstrating the studied cross-linking reaction is a time dependent process. Giving more time to the reaction provides further reaction between the functionalities and results in relatively higher reaction enthalpy and lower peak temperature. The reaction enthalpy is increased from 20.5 to 31.2 J/g while the maximum temperature of the exothermic peak is decreased from 144.3 to 133.5 °C by reducing the heating rate from 20 to 10 °C/min.

The dependence of the T_g of the nanocomposites on composition was illustrated in Fig. 7. The glass transition temperature of OP-POSS is about 15.5 °C and the corresponding values for the nanocomposites having 10, 25, 40, 50, and 60 wt% of MWCNT–COOH were found to be 17.3, 21.8, 19.4, 18.2, and 21.2 °C, respectively. As compared with OP-POSS, the OP-POSS/MWCNT–COOH nanocomposites possess relatively higher T_g as a result of the cross-linking reaction. For the nanocomposite with 25 wt% of MWCNT–COOH, the contribution from the cross-linking reaction is the highest. Higher availability of MWCNT–COOH causes esterification reaction to be progressed effectively. However, it is difficult to produce completely homogeneous mixtures having very high loading of MWCNT–COOH into OP-POSS matrix due to tendency of MWCNT–COOH to form aggregates. These aggregates would act as barriers for the cross-linking reaction at nanoscale.

3.3. WAXD observations

The structure of the nanocomposites was further investigated by wide-angle X-ray diffraction (WAXD) as shown in Fig. 8. For comparison, the pattern of MWCNT–COOH was also presented. The WAXD pattern of the MWCNT–COOH has only one main clear reflection at 2θ of 25.4°. The WAXD patterns of all the nanocomposites display a relatively broad peak at 2θ of 16.9° corresponding to an amorphous phase. Therefore, the WAXD data give obviously no indication of the presence of crystalline POSS aggregate in the produced nanocomposites even when the mass fraction of the OP-POSS was as high as 60%. In our previous study, we demonstrated that the OP-POSS is a liquid amorphous material with two amorphous halos at 24.1° and 17.5° [44]. Therefore, it may be implied that the peak at 16.9° is due to the presence of un-reacted OP-POSS. But, we believed that contributions from un-reacted OP-POSS and cross-linked amorphous nanostructures must be taking into account simultaneously to appear this band especially for the blends with low MWCNT concentrations. If this peak could only be assigned to un-reacted OP-POSS, its intensity should be the highest for the nanocomposite having the lowest amount of MWCNT, i.e. 10%. Clearly, this fact was not observed in Fig. 8.

On the other hand, by decreasing the concentration of OP-POSS in the blends the intensity of the peak at 16.9° was increased. More interestingly, this phenomenon was not significant in the nanocomposite involving 60% MWCNT. This could be described according to the fact that at high MWCNT concentrations, the self-aggregating effect must be significant. Therefore, the effectiveness of the nanocross-linking reaction will be limited by two factors: low concentration of OP-POSS and aggregation of MWCNT which, indeed, restricts free COOH functionality available for esterification reaction. However, because of the limited sensitivity of WAXD, the occurrence of some clustering of OP-POSS units or phase-separated small-sized inorganic domains cannot be ruled out.

3.4. Surface morphology by optical microscopy and AFM measurements

Atomic force microscopy (AFM) was used to characterize both the sole functionalized MWCNT and OP-POSS/MWCNT nanocomposites. The AFM topographical images of the pure MWCNT and nanohybrids were presented in Fig. 9. The AFM images reveal a surface characterized by a network of cylindrical-like features with lengths of several hundreds of nanometers and much smaller width. These lines represent the segments of the MWCNT that approach the surface and confirm a random planar arrangement. The height and phase contrast images showed that the presence of some voids and zones of different packing density. The topographic line scans indicate a roughness with a maximum peak-to-valley distance of up to 300 nm in the case of nanocomposites.

We attempted analyzing the roughness of the produced nanostructures in details and results were shown in Fig. 10. As it can be seen, the surface roughness of the cross-linked nanostructures is influenced by the blend composition and was higher for the nanocomposites having higher values of MWCNT. The OP-POSS/MWCNT (10%) nanocomposite exhibited a smoother featureless surface (lower root mean square roughness, RMS), while the blends containing higher percentages of MWCNT, i.e. 40% and 60%, showed raised features possibly attributed to MWCNT aggregates and crystallites. Also, the nanocomposites samples exhibited relatively large raised and elongated surface features, higher radius diameter with MWCNT concentration, as a result of nanocross-linking reaction.

From AFM images of the nanocomposites, the surface roughness profiles vary from 55.8 to 104.4 nm and it increases with increasing MWCNT concentration. Typically, OP-POSS at MWCNT (10%) results in a roughness of 55.8 nm and OP-POSS at MWCNT (40%) has a roughness of 90.7 nm. Therefore, as the concentration of the COOH functionality on MWCNT surface increased, a larger nanoscale structure is formed that might be attributed to cross-linking reaction. Moreover, the size of the nanostructure was influenced by the reactivity of the functional groups of MWCNT as well as by the steric hindrance from the phenol groups of the OP-POSS. It is worthy to notice that the changes in nanoscale roughness associated with MWCNT concentration are related to the values of T_g. As the surface roughness is increased above a certain threshold value, the values of T_g decreased as previously observed from the DSC measurements. In conclusion, the AFM results indicate that the grafted groups on the MWCNT can affect the roughness.

4. Conclusions

The multiwall carbon nanotube (MWCNT)/polyhedral oligomeric silsesquioxane (POSS) nanocomposites were successfully prepared by the direct esterification between carboxylic acid functionalized multiwall carbon nanotube and octa(phenol) octasilsesquioxane (OP-POSS). The solubility and processability of MWCNT–COOH in organic solvents are substantially improved because of the specific role that OP-POSS plays in dispersing MWCNT–COOH. The glass transition temperature (T_g) of the OP-POSS/MWCNT nanocomposites was higher than that of the OP-POSS as the result of cross-linking reaction. Also, cross-linking via a simple reaction results in improvement of the OP-POSS thermal stability and roughness as evidenced by TGA and AFM observations.

References

[1] R.I. Gonzalez, S.H. Phillips, G.B. Hoflund, J. Spacecraft Rockets 37 (4) (2000) 463.
[2] G.B. Hoflund, R.I. Gonzalez, S.H. Phillips, J. Adhes. Sci. Technol. 15 (10) (2001) 1199.
[3] W.Y. Chen, Y.Z. Wang, S.W. Kuo, C.F. Huang, P.H. Tung, F.C. Chang, Polymer 45 (20) (2004) 6897.
[4] R.M. Laine, C. Zhang, A. Sellinger, L. Viculis, Appl. Organomet. Chem. 12 (10–11) (1998) 715.
[5] F.J. Feher, D.A. Newman, J.F. Walzer, J. Am. Chem. Soc. 111 (1989) 1741.
[6] R. Duchateau, H.C.L. Abbenhuis, R.A. van Santen, A. Meetsma, S.K.H. Thiele, M.F.H. van Tol, Organometallics 17 (25) (1998) 5663.
[7] C.C. Cheng, C.H. Chien, Y.C. Yen, Y.S. Ye, F.H. Ko, C.H. Lin, F.C. Chang, Acta Mater. 57 (6) (2009) 1938.
[8] A. Provatas, M. Luft, J.C. Mu, A.H. White, J.G. Matisons, W. Brian, B.W. Kelton, J. Organomet. Chem. 565 (1–2) (1998) 159.
[9] F.J. Feher, Silicon Compounds: Silanes & Silicones, Gelest, Inc, PA, USA, 2004.
[10] D.A. Armitage, Inorganic Rings and Cages, Edward Arnold Ltd., London (UK), 1972.
[11] E.O. Dare, L.K. Liu, J. Peng, J. Chem. Soc. Dalton T. 30 (2006) 3668.
[12] H. Liu, S. Zheng, K. Nie, Macromolecules 38 (14) (2005) 5088.
[13] J. Choi, A.F. Yee, R.M. Laine, Macromolecules 36 (29) (2003) 5666.
[14] G.S. Constable, A.J. Lesser, E.B. Coughlin, Macromolecules 37 (4) (2004) 1276.
[15] Y. Ni, S. Zheng, Macromolecules 40 (19) (2007) 7009.
[16] P.P. Pescarmona, J.C. Van der Waal, T. Maschmeyer, Chem. – Eur. J. 10 (7) (2004) 1657.
[17] R. Duchateau, H.C.L. Abbenhuis, R.A. Van Santen, S.K.H. Thiele, N.F.H. Van Tol, Organometallics 17 (1998) 5222.
[18] V. Lorenz, S. Giebmann, Y.K. Gun'ko, A.K. Fischer, J.W. Gilje, F.T. Edelmann, Angew. Chem. Int. Ed. 116 (2004) 4703.
[19] H. Liu, S. Kondo, R. Tanaka, H. Oku, M. Unno, J. Organomet. Chem. 693 (7) (2008) 1301.
[20] A.R. Bassindale, M. Pourny, P.G. Taylor, M.B. Hursthouse, M.E. Light, Angew. Chem. Int. Ed. 42 (30) (2003) 3488.
[21] H.M. Lin, K.H. Hseih, F.C. Chang, Microelectron. Eng. 85 (7) (2008) 1624.
[22] I.A. Zucchi, M.J. Galante, R.J.J. Williams, E. Franchini, J. Galy, J.F. Gerard, Macromolecules 40 (4) (2007) 1274.
[23] C. Zhang, R.M. Laine, J. Am. Chem. Soc. 122 (29) (2000) 6979.
[24] D. Neumann, M. Fisher, L. Tran, J.C. Matisons, J. Am. Chem. Soc. 124 (2002) 13998.
[25] R. Tamaki, Y. Tanaka, M.Z. Asuncion, J. Choi, R.M. Laine, J. Am. Chem. Soc. 123 (2001) 12416.
[26] C.M. Brick, R. Tamaki, S.G. Kim, M.Z. Asuncion, M. Roll, T. Nemoto, Y. Ouchi, Y. Chujo, R.M. Laine, Macromolecules 38 (11) (2005) 4655.
[27] C.M. Brick, Y. Ouchi, Y. Chujo, R.M. Laine, Macromolecules 38 (11) (2005) 4661.

[28] C.M. Brick, E.R. Chan, S.C. Glotzer, J.C. Marchal, D.C. Martin, R.M. Laine, Adv. Mater. 19 (1) (2007) 82.
[29] Y.C. Yen, S.W. Kuo, C.F. Huang, J.K. Chen, F.C. Chang, J. Phys. Chem. B. 112 (35) (2008) 10821.
[30] Y.C. Yen, Y.S. Ye, C.C. Cheng, H.M. Chen, H.S. Sheu, F.C. Chang, Polymer 49 (17) (2008) 3625.
[31] P. Singh, S. Campidelli, S. Giordani, D. Bonifazi, A. Bianco, M. Prato, Chem. Soc. Rev. 38 (8) (2009) 2214.
[32] S. Banerjee, T. Hemraj-Benny, S.S. Wong, Adv. Mater. 17 (1) (2005) 17.
[33] J.N. Coleman, U. Khan, Y.K. Gun'ko, Adv. Mater. 18 (6) (2006) 689.
[34] F. Dalmas, L. Chazeau, C. Gauthier, K. Masenelli-Varlot, R. Dendievel, J.Y. Cavaillé, L. Forró, J. Polym. Sci. Part B: Polym. Phys. 43 (10) (2005) 1186.
[35] B.S. Shim, P. Podsiadlo, D.G. Lilly, A. Agarwal, J. Leet, Z. Tang, S. Ho, P. Ingle, D. Paterson, W. Lu, N.A. Kotov, Nano Lett. 7 (11) (2007) 3266.
[36] I. O'Connor, H. Hayden, J.N. Coleman, Y.K. Gun'ko, Small 5 (4) (2009) 466.
[37] G.X. Chen, H. Shimizu, Polymer 49 (4) (2008) 943.
[38] K. Xie, Y. Zhang, Y. Yu, Carbohyd. Polym. 77 (4) (2009) 858.
[39] T. Morishita, M. Matsushita, Y. Katagiri, K. Fukumori, Carbon 48 (8) (2010) 2308.
[40] B. Zhang, Y. Chen, J. Wang, W.J. Blau, H. Zhuang, N. He, Carbon 48 (6) (2010) 1738.
[41] H.C. Lin, S.W. Kuo, C.F. Huang, F.C. Chang, Macromol. Rapid. Commun. 27 (7) (2006) 537.
[42] M.A. Karakassides, D. Gournis, D. Petridis, Clay Miner. 34 (3) (1999) 429.
[43] G. Lu, Y. Huang, Y. Yan, T. Zhao, Y. Yu, J. Polym. Sci. Part A: Polym. Chem. 41 (16) (2003) 2599.
[44] Y.C. Sheen, C.H. Lu, C.F. Huang, S.W. Kuo, F.C. Chang, Poymer 49 (18) (2008) 4017.